Simulation on the structure of pig liver esterase

Daniel Hasenpusch, Uwe T. Bornscheuer, Walter Langel

Abstract graphic

Click here to download high resolution image

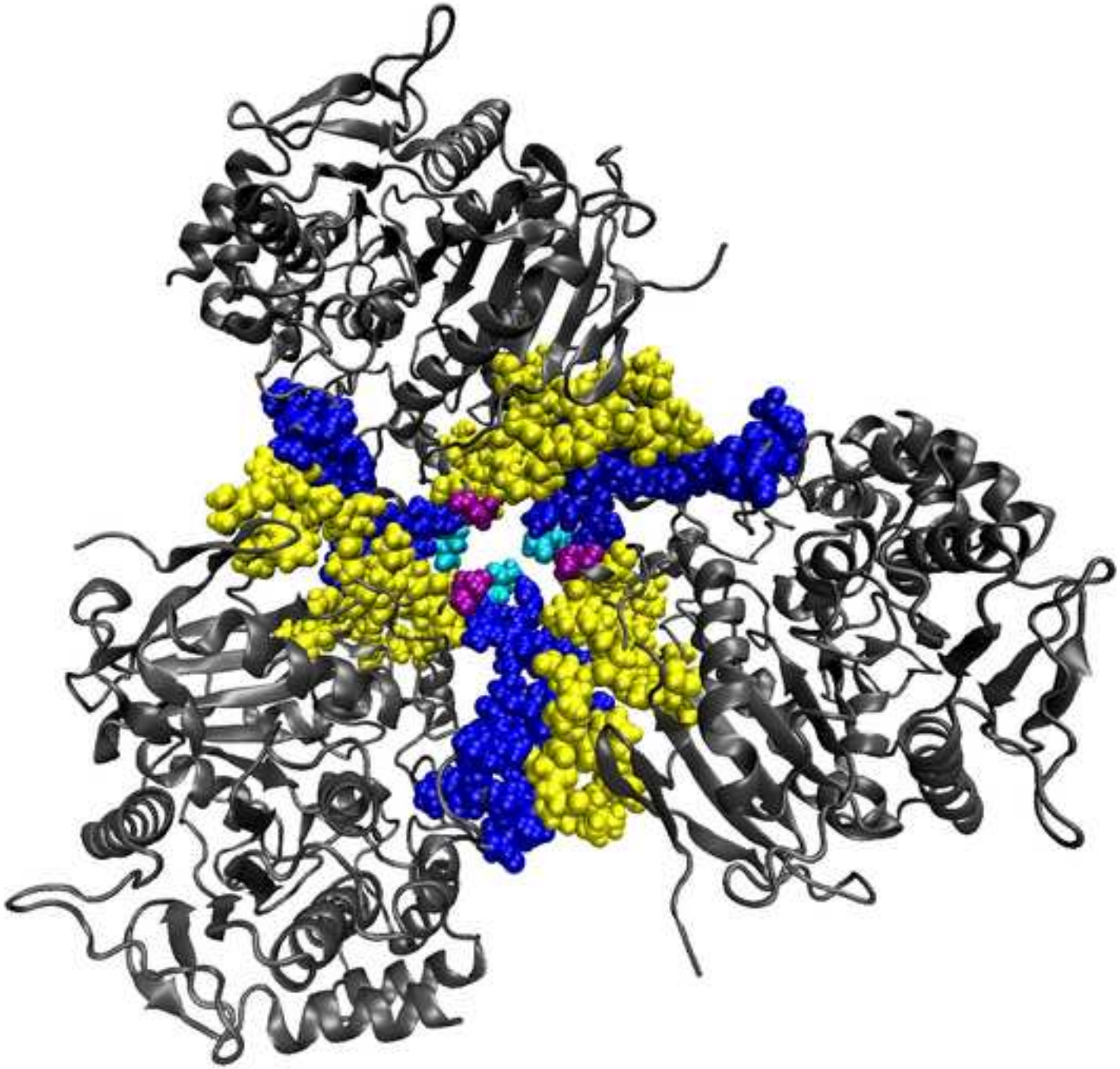

Simulation on the structure of pig liver esterase

Received: 22.02.2010 / **Accepted:** 01.09.2010

Daniel Hasenpusch[1], Uwe T. Bornscheuer[2], and Walter Langel[1,✉]

[1] Department of Biophysical Chemistry, Institute of Biochemistry, University of Greifswald, Felix-Hausdorff-Str. 4, 17487 Greifswald

[2] Department of Biotechnology & Enzyme Catalysis, Institute of Biochemistry, University of Greifswald, Felix-Hausdorff-Str. 4, 17487 Greifswald

✉Email: langel@uni-greifswald.de

Abstract

A homology model for pig liver esterase was generated on the basis of human carboxyl esterase (hCE) and subjected to extensive molecular dynamics simulations. By virtual mutations the isoenzymes PLE1-6 and APLE were obtained, and the PLE1 trimer was built from the respective model of hCE. Stable structures for all systems were attained after simulations in solution for 12-18 ns, and contact zones between the monomers in the trimer are described. By evaluation of RMSD values of the residues in the monomer a rigid backplane with a number of β-strands and a flexible front part containing several α helices are distinguished. All mutations are concentrated in the soft part, and significant differences in the folding states of the helices were distinguished between the isoenzymes. Substrate access to the active site passes through two helices whose structures are affected by mutations. Variations in substrate specificity between the isoenzymes are ascribed to the structure of the entrance channel rather than to the conformation of the active site itself.

The assignment of the residue with a negative side chain stabilizing the histidine protonation in the catalytic triad was revised, being GLU 452 in some isoenzymes rather than GLU 336, which would be the correspondent to most hydrolases. Arguments for this new assignment are given on the basis of simulations and statistics from the 3DM database for hydrolases.

Keywords Carboxyl esterases · Pig liver esterase · Molecular dynamics · Force field

Introduction

Pig liver esterase (PLE) is widely used as biocatalyst in organic synthesis [1]. The enzyme was studied in detail for the last 30 years and many applications were described [2]. The conversions of a broad range of racemic or prostereogenic esters proceed with high to excellent enantioselectivity, making PLE a very useful enzyme for sophisticated organic synthesis processes.

Typically the active sites of serine hydrolases is a catalytic triad with a SER, a HIS, and an ASP or GLU residue [1]. The side chain carboxyl group of ASP/GLU polarizes the adjacent HIS, which in turn accepts the hydroxyl proton from SER during the catalytic reaction. In early work the residues SER 200, HIS 440, and GLU 327 were assigned to the active triad of the acetylcholine esterase from *Torpedo californica* (TcAChE [3]). This was confirmed for further acetylcholine esterases by proving that the analogous GLU residue is essential for catalytic activity [4]. Analogous assignments were made for lipases such as *Candida rugosa* Lipase (CRL) [5]. In contrast to that the orientation of the side chain of the analogous GLU 353 residue in rabbit carboxyl esterase (rCE) (pdb codes 1THG and 2BCE [6]) is opposite to that found for other esterases, and it is unlikely that this GLU 353 stabilizes the HIS 467 of the rCE active site.

No crystallization and crystal structure determination of pig liver esterase (PLE) was possible so far. The folding states of parts of the sequence to α and β structures were assigned in analogy to known structures of typical **α, β–hydrolases** [1, 7]]. Originally three isoenzymes (α, β, γ) with different sequences and substrate specificities had been characterized in [8, 9]. The γ-isoenzyme of the PLE initially identified as proline-β-naphthyl amidase was cloned and overexpressed in *P. pastoris* X33 [10] and *E.coli Origami* [11]. In 2008 additional isoenzymes were identified, and the amino acid sequence of six of them was determined. They differ by a small number of mutations (Table 1) and were denoted PLE1-5 [12]. PLE1 is identical to the former γ-PLE, whereas no unique assignment of the former α and β modifications was possible. In [13] the sequence of an additional modification, PLE6, is given. A further isoenzyme which complements the mutation pattern of PLE3 and PLE5 was described as alternative PLE (APLE) [14]. Determination of the molecular weight has shown that under physiological conditions the enzyme mostly forms trimers which contain a random combination of different isoenzyme monomers [8, 9].

In this paper we focus on 3D models for the enzyme structure without deformation by an embedded substrate as a first step towards understanding the reaction mechanism of the enzyme and its enantioselectivity. As the geometry of the active site might be modified by trimerization, we generated models of both monomer and trimer. A wide spread and valid method for generating 3D models of poorly crystallizing enzymes is homology modeling. The PLE1 has a high sequence homology (about 75%) to human liver carboxyl esterase (hCE) and rabbit liver esterase (rCE) whose crystal structures are known.

The structural basis of heroin and cocaine metabolism was also reported based on the crystal structure of hCE [15] and a possible entrance path to the hidden active site in hCE was described. Here, we verified the feasibility and stability of the homology model by extensive molecular dynamics simulations on the monomer. The originally modeled PLE1 was modified by several mutations transferring it to other isoenzymes. We traced the influence of single mutations and extended sequence variations on the secondary structure by classical molecular dynamics. This afforded extended simulations, since local rearranging and especially modification of the folding state around a newly introduced mutation may occur on a time scale of several ns, which was beyond the scope of earlier work. By runs of similar lengths the contacts between the trimeric subunits were characterized.

Methods

A homology model [16] of the PLE1 isoenzyme was generated on the basis of the human carboxyl esterase [17]. As a template we used the X-ray structures of hCE complexes with the heroin analogue naloxone methiodide (1MX9, chain A). The rabbit liver esterase rCE [6] has an even greater similarity to PLE than hCE, but the only available crystal structure of its complex with 4-piperidino-piperidine (1K4Y) contains three hypervariable loops close to the active center, and 33 amino acids could not be localized. The full PLE sequence (molecular weight about 60 kDa) starts with a signal peptide with 18 residues, which is cleaved during processing of the enzyme. During homology modeling the sequence GQP at the N-terminus and ten residues in addition to the ER-retention signal HAEL at the C-terminus were omitted. According to standard numbering our models contains the PLE residues 4 to 534.

For the isoenzymes PLE2-6 and APLE the respective side chain atoms of the mutated residues in the optimized PLE1 structure were stripped, and their names in the pdb file

replaced. This data set was reloaded into the xLeap program of the AMBER package (versions 7 to 10) [18], which adds the missing side chain atoms of the mutated residues according to predefined standard structures of the respective amino acid.

The crystal structure of human carboxyl esterase trimers in complex with taurocholate (2DR0) was used as a template for the PLE trimer, and three identical PLE1 monomers from a trajectory with 6 ns simulation time were aligned to each of the three chains of this model. No hydrogen bonds between the PLE1 monomers were predefined in this initial configuration. The 531 residues in the identical monomers are denominated 4-534/1, 4-534/2 and 4-534/3.

Molecular dynamics simulations

Models for molecular dynamics simulations were prepared in xLeap using the parm94 force field. Orthorhombic box dimensions for periodic boundary conditions were 72x84x92 $Å^3$ and 85x137x134 $Å^3$ for single monomers and trimers, respectively. This allowed for a spacing of at least 10 Å between enzyme and cell boundaries. The box was filled with about 50000 and 40000 discrete TIP3P water molecules for monomers and trimers, respectively. Bond lengths of the water molecules were fixed using a SHAKE algorithm. Under physiological conditions all proteins considered here had negative total charges, which were compensated by appropriate addition of Na^+ counter ions (CIO) to the system.

The geometry of each system was optimized during at least three runs, relaxing (1) the positions of the water molecules and the counter ions, and (2) the enzyme structure only in fixed water environment, and (3) minimizing the energy of the whole system. Starting structures for all mutations were derived from the homology model of PLE1 after geometry optimization. By molecular dynamics at constant pressure and temperature (NpT) for 20ps cell size and water density were adjusted. Production runs scanned 14 ns at constant energy with an initial temperature of 300 K and a time step of 1 fs. All images of 3D structures were generated with VMD [19] and its plug-ins [20-23].

Conclusions from our simulations on a limited number of structures were cross checked by comparison with super families of proteins with related sequences and functions. The database program 3DM allows data to be organized around a single class of molecules, and a common numbering scheme for structurally equivalent amino acids is used enabling the identification of conserved residues and distributions of amino acids for specific residues.

First a subfamily of mammalian carboxyl esterases similar to PLE and hCE was derived from the full **α/β folded hydrolases superfamily** with about 12000 structures. This subfamily contained about 170 structures, but showed only a small number of 3DM core residues, for which conservation statistics may be evaluated. The **superfamily** comprises a wide spectrum of different structures with little overlap. We cured this problem by starting from a **family** of about 1300 structures around the prototype acetylcholine esterase. Subfamilies such as lipases are now omitted, and the members of the acetylcholine esterase **family** are much more similar to each other than those of the **superfamily**. Consequently the number of 3DM core amino acids is much higher in this new **family**. Still its **subfamily** with PLE and hCE has nearly as many members (150) as the one derived from all **α/β folded hydrolases** with known 3D structure.

Results and discussion

Monomer structure, mutations and their position relative to the entrance helix

The secondary structure of the nearly globular protein (Fig. 1) consists of a series of α helices and β-folds. The residues in the range 72-87 are referred to as entrance helix. In contrast to the lipases the active site is not freely accessible in all esterases, and substrates have to pass between this α helix and its counterpart, formed by residues 338-346. Folding in this range thus is crucial for the formation of the Michaelis-Menten complex and for the activity of the enzyme.

The 25 mutations between the isoenzymes are correlated in part forming six independent groups (Table 1 and Fig. 2). The β-folds are highly conserved and not affected by any of the mutations considered here:

(1) For residues 73, 75-77, 80 on the entrance helix, three combinations are possible, (i) ASP, VAL- VAL-GLU, THR (ii) ASP, VAL- ALA-GLY, THR or (iii) GLU, ILE- GLY-GLY. LEU. ASP and VAL or GLU and ILE on positions 73 and 75 are pair wise correlated. Very important for the stability of the helix should be the transition from VAL and GLU to GLY or ALA on position 76 and GLY on 77, respectively.

(2) Eleven mutations in three different strands are strictly correlated: 87, 92 and 93 are close to the entrance helix. 129, 133, 134, 138 and 139 are on a strand which is parallel to the entrance helix and has partial helix folds. Residue 138 is close (within 5 Å) to 139 and 462. The residue 139 in turn is near to 461 and 462 and can interact with 461 directly. This may affect the positions of 459 and 463 and have an indirect influence on the structure of the entrance helix. 234, 236 and 237 have distances of more than 7 Å to the entrance helix, and no obvious correlation between their configuration and the structure of the entrance helix was found.

Three further groups of mutations, (3-5) are found on a single strand between residues 285 and 302:

(3) The only uncorrelated single point mutation transfers PHE on position 285 to PRO and might affect the residues 286 and 287 next to the entrance helix.

(4) For 286 and 287 the sequences LEU-THR or PHE-ALA were found, which mainly differ by an exchange of the aliphatic and aromatic side chains.

(5) A triple mutation on 290, 294 and 302 in the same strand as groups (3) and (4) transfers PHE, GLN, PRO into LEU, PRO, THR. Amino acid 290 is close to the loop of 285 to 287 and its mutation may have an impact on the substrate entrance. Two further mutations shift a proline from position 302 to 294. This switches the ω-angles at both positions by 180° and will essentially rotate the very flexible backbone structure between them by 180°. Outside of this window 294 to 302, the effects of both mutations on the backbone conformation probably compensate to a wide extent.

(6) The group of three mutations on the positions 459, 461 and 463 transfers PHE, LEU, LYS into ALA, PHE, ARG shifting the aromatic side chain from 459 to 461. This might deform an α-helix in the proximity of the entrance helix.

RMSD of the monomer

Root mean square displacements (RMSD) of the coordinates of single residues were evaluated by comparing the atomic positions in the last frames of the total simulation time of 14 ns with those every 2 ns before, for trajectories (Fig. 3) from the seven PLE isoenzyme

monomers (PLE1-6 and APLE) as well as the three PLE1 monomers in the trimer. MD calculations induced significant relaxation in most parts of the secondary structures derived from geometry optimized PLE1. Typically initial RMSD values of 5-10 Å decreased to 1-3 Å during the interval from 8 to 12 ns (Fig. 3a). This indicates relaxation of the mutated parts and a stabilization of the whole isoenzyme. Only during the last 2-4 ns the RMSD value further decreased due to convergence of the structure to the final configuration. In some cases fluctuations with periods of 2-5 ns were observed which may be due to slow rearranging of larger structures of the enzyme (Fig. 3b).

The impact of the mutations on the final isoenzyme structures was analyzed by using in turn one of them as template and evaluating the RMSD for the others. In major parts of the isoenzymes, mutations incite little rearranging and fluctuation, and the RMSD values between different isoenzymes were below 2 Å, in part even below 1 Å. All β-folds and a few helices form a rigid and highly conserved backplane of the enzyme, which is its basic structure (Fig. 4). In contrast to that the flexible front consists of a major part of the helices and of several loops, containing all mutations. Many variable structural elements strongly affect the enzyme structure, especially near the entrance and around the active site (Fig. 5a).

Influence of the mutations on the structure of the enzyme

In the isoenzymes considered here, the entrance helix is affected by up to five mutations with respect to PLE 1 (Fig. 2), and some of them are known to affect the experimental substrate specificity (e.g. VAL to ALA and GLU to GLY on positions 76 and 77, respectively [24]). With the exception of PLE3, (Fig. 5b, Fig. 6), the residues 74-83 form a well-defined α-helix (Fig. 5a, *yellow*). In this isoenzyme the dihedrals for four residues (74, 75, 77 and 80) are not in the range of α-folds, and the helix is broken into a coil structure. We speculate that this is a collective effect of the mutations in groups (1) and (3). The replacement of residues 76 and 77 by glycines certainly weakens the entrance helix, but this has no effect on its folding in PLE6 and APLE. If the additional mutation of residue 285 into a proline shifts the helix (272 to 284), some stress on the entrance helix might induce unfolding.

The residues 89-96 formed a random coil in the homology model and in most isoenzymes but arranged to a short helix in the PLE1 monomer (Fig. 7). This folding is reflected by high RMSD values above 6 Å very close to the entrance helix (*blue* in Fig. 4). The secondary

structure of this flexible zone seems to be the result of a complicated interplay of several mutations.

Trimer

The trimer built from three PLE1 monomers has a propeller like structure (Fig. 8) and is stable during the simulation time of 14 ns. The rigid and soft parts of the monomers are found on the bottom and on the top of the propeller blades, respectively. All three interfaces between the trimers have similar structures involving nearly the same corresponding residues (Table 2). The contact site between subunits 1 and 2 is shown in detail in Fig 8 *(insert)*. The residues are contained on three and four strands for the clockwise (Table 2a) and counterclockwise oriented monomer faces (Table 2b), respectively.

The PLE monomers contain five cysteine residues which form two **disulfide-bridges** (70-99, and 256-267) close to the contacts between trimer subunits (cf. Table 2). According to [25], residue 70 rather than the adjacent CYS 71 is involved in the first bridge. It is conserved to 100% in the **subfamily** of PLE, and this high degree of conservation indicates substantial importance for the enzyme structure. We assume that it maintains the connection between the strands 5' and 6' (*red* and *orange* in Fig. 8), whereas 256-267 close a loop inside strand 2 (*blue*). The cystine bridges seem to stabilize the contact areas between the subunits and thus may be essential for trimerization.

The RMSD pattern of the final structure of the trimer was obtained by comparing the amino acid in each of the three monomers with their correspondents in the relaxed PLE1 configuration, from which the trimer had been assembled. Deviations in the RMSD pattern between the trimer components and monomer PLE1 are similar as between the mutated and original monomers.

Assignment of the catalytic triad and structure of the active site

SER 204 has been identified earlier as the nucleophilic residue in the active site, and the acceptor for its proton is HIS 449. The two tautomeric forms δ and ε of histidine with the N_δ and N_ε atoms protonated, respectively, are equilibrated at physiological pH-values by proton transfers [26]. This cannot be reproduced in a force field calculation, and AMBER

provides three predefined residues, HID, HIE, and HIP, denoting the δ– and ε-tautomers and the doubly protonated form of the imidazol ring, respectively. According to the homology model, only a proton at N_δ points towards negatively charged oxygen atoms, whereas an H atom at the ε-species would be directed versus the SER hydroxyl group hindering proton transfer from SER to HIS. Rotation of the ring around the C_α-C_β bond by 180° does not cure this problem, since the two N-atoms are not in symmetrical positions with respect to this axis. We used the δ-tautomer (HID) as residue 449 enabling the formation of a very stable hydrogen bond between the O_γ of SER 204 and the deprotonated histidine N_ε. The O_γ from SER 204 can also be stabilized by GLU 229 and GLU 203, the H_γ proton forming transient H-bonds to the backbone O of these residues (Fig. 9). The hydrogen bonds to HIS 449 and to GLU 229 are alternating during simulation.

The protonated N_δ of HIS 449 forms hydrogen bonds to negatively charged atoms. The previous assignment [4, 6] provides stabilization by the GLU 336 side chain. In none of the present simulations this group pointed to the active site, and no stable hydrogen bonds to HIS 449 were formed. In most PLE structures the carboxyl O atoms of the GLU 336 side chain had distances of about 8 Å to the HIS N_ε after molecular dynamics. The group is oriented into the opposite direction forming stable hydrogen bonds to LYS 521 NZ or backbone N atoms of GLU 336, LYS 334 and ASN 333. For the bonding in the active site we distinguish three different patterns:

(1) In PLE1, PLE2 and APLE the carboxyl group of GLU 452 is close to the protonated N_δ atom of HIS 449 with O-N-distances of less than 3 Å, forming very stable hydrogen bonds. The side chain carboxyl group reorients in some cases and alternating bonds to $O_{\varepsilon 1}$ and $O_{\varepsilon 2}$ are observed. When assuming that GLU 336 is replaced by GLU 452 in the catalytic triads, the two characteristic distances between SER and HIS, as well as HIS to GLU have the typical values, and the exchange should have small impact on the catalytic mechanism.

(2) In PLE4 and PLE6 the HIS 449 ring rotates by 180° around the C_α – C_β axis. Still the H-bond between SER 204 Oγ and HIS 449 N_ε is stable, but the proton at N_δ forms an H-bond to backbone GLU 336 O.

(3) The active sites of PLE3 and PLE5 differ from those of the other isoenzymes. Even though PLE3 formed stable hydrogen bonds between HIS 449 N_δ and GLU 452 OE1 or OE2,

the N_ε of HIS 449 and the O_γ of SER 204 were too far apart for a hydrogen bond. The SER 204 is rather stabilized by the GLU 229 backbone O. PLE 5 has only one stable H-bond in the catalytic triad between the two protonated atoms HIS 449 N_δ to SER 204 O_γ, since the histidine ring is stuck in a position which makes the formation of the expected H-bond to HIS 449 N_ε impossible.

In all isoenzymes but PLE5 and PLE6 the carboxyl group of GLU452 is fixed by additional hydrogen bonds and has a stable position. One of the carboxyl oxygen atoms, $O_{\varepsilon1}$ or $O_{\varepsilon2}$, is hydrogen bonded to backbone N atoms of GLY 450, ASP 451 and GLU 452. The second oxygen, $O_{\varepsilon2}$ or $O_{\varepsilon1}$, forms hydrogen bonds to ASN 333 ND2 and SER 230 O_γ in all runs. GLU 336 and GLU 452 are cross linked via ASN 333, and their side chain orientations are correlated. In PLE5 the respective distances are elongated to 3-4 Å, whereas in PLE6 the side chain of 452 has reoriented.

Molecular mechanics calculations depend on the parameterization of the respective force field. We verified if the reorientation of the GLU 336-GLU 452 is an artifact of the force field used here. In the experimental structures of rCE [6] the side chains of the two residues equivalent to 336 and 452 are oriented towards the HIS equivalent to 449 in PLE, but neither carboxyl group is close enough to the proton at N_δ for a hydrogen bond. Due to the missing positions for 33 residues, rCE could not be used as starting structure. We instead simulated four hydrolases, for which the active centers are fully known: hCE (1MX9), TcAchE (2VJA), aged form of human butyrylcholinesterase (hBuChE, 2WSL), and CRL (1LPM). The same protocol as for PLE was used and in the unconstrained simulations all enzymes had stable hydrogen bonds between their HIS N_ε and SER H_γ in the active sites (Table 3a). In each case except of TcAchE alternative bonding of the SER H_γ proton to second acceptors was also observed. They mostly consisted of a backbone O of GLU 229 (PLE), SER 222 (hBuChE), and GLY 123 (CRL), or a side chain carboxyl group of GLU 200 (hCE), Only in the case of hBuchE this alternative hydrogen bond was more stable than the SER-HIS contact.

In the experimental structure of hCE [17], GLU 334 (equivalent to position 336 in PLE) forms a weak hydrogen bond (3 Å) to HIS 447 (equivalent 449). After a very short simulation time of only 100 ps this GLU relaxes and a hydrogen bond to GLU 450 (equivalent 452) is formed, which is close to HIS 447 already in the starting configuration (Table 3c). In unrestrained simulations of TcAChE, hBuChE and CRL, histidine in the active site is

stabilized by the GLU residue equivalent to 336, and the calculation confirms the assignment given in the literature [3, 4, 6, 27-29] for the majority of hydrolases (Table 3b). We thus obtained a stable active site with the equivalents of GLU 336 and HIS 449 bonding for at least three hydrolases from our simulation protocol, whereas in an early force field calculation over just 400 ps this structure could only be stabilized by restraints [5]. This makes it unlikely that the AMBER force field parametrization artificially induces the switching from GLU 336 to GLU 452 in PLE.

Interpretation of the results on the basis of the 3DM database

According to [30], GLU 452 is conserved and has a crucial importance. The survey with 3DM supported quantitatively the high conservation of amino acids at the core position equivalent to 452 in PLE. In the AChE **family** 63.2% GLU / 33.8 % ASP and in its **subfamily** 62.4% GLU / 35.6% ASP were found. In the hydrolases **superfamily** this position is no core residue indicating that it has specific importance in the AChE **family,** but not in all other members of the **superfamily.** It would be consistent with our simulations if this residue was part of the active site in most members of the AChE **family**, but not of the **superfamily**.

In contrast to that the position 336 in PLE is highly conserved in the **superfamily** having scores of 74.4% ASP / 19.9% GLU. As ASP is prevailing at this position, the mechanism of hydrolysis is in general described with this amino acid in the catalytic triad. Whereas GLU in this position is an exception in the **superfamily**, it is nearly quantitatively found in the respective positions in the acetylcholine **family** (91.2 % GLU / 6.7% ASP) and in its **subfamily** (96.0% GLU and 2.6% ASP).

Mutations affecting the orientations of GLU 336

Two differences between the sequences in the acetylcholinesterase **family** and in its **subfamily** of mammalian esterases with hCE and PLE might contribute to the flip of the GLU 336 side chain:

(1) The PLE **subfamily** preferably contains a LYS at position 521 instead of ARG in acetylcholine and butyrylcholine esterases. The ARG side chain forms a very stable salt bridge to ASP 404, which is a highly conserved residue in both families (98.7 % and 80% in the **subfamily** and the acetylcholine **family**, respectively). The link between residues 404 and

521 is weakened by replacing ARG with LYS, and the LYS side chain can form a hydrogen bond to the reoriented GLU 336 side chain. This was not possible in enzymes with ARG at position 521.

(2) At the positions 337 and 338 next to GLU 336, significant differences are found between **family** and **subfamily**. In the acetylcholineesterase **family** GLY is dominant on position 337 (65.9%), where only 4.0% of the members of the **subfamily** have a GLY residue, PHE being favored (63.6%). At the neighboring position 338 the situation is reversed with 11.3 % and 87.3 % of glycine in the AChE **family** and its **subfamily**, respectively. This position is not conserved in the AChE **family**, and several other amino acids than GLY could be located here, mainly LEU, THR and SER with frequencies of 20.1, 18.4 and 13.6%, respectively. Shifting of GLY by one position from the neighbor of the glutamic acid in the AChE-**family** to the second residue after GLU 336 in PLE, might modify the flexibility of the strand close to GLU 336 and favor the reorientation of its side chain away from the active site.

Exchanging only these two amino acids, as suggested by results from the 3DM-evaluation (PHE337GLY and GLY338THR) did not have significant influence on the orientation of the GLU 336 side chain in a further simulation, and additional differences in the sequences between **family** and **subfamily** should be relevant: The residues 337-346 were replaced with two corresponding sequences from other hydrolases including the 10 amino acids following the glutamate/aspartate residue corresponding to GLU 336 in PLE. In these enzymes it is known that this residue indeed is part of the active site. The first sequence contained typical residues for choline esterases (Fig. 10, Mutation 1) and the second one was taken from CRL (Fig. 10, Mutation 2). In the homology model used as starting configuration the side chain of GLU 336 is oriented towards HIS 449. First a reorientation like in PLE1 was observed, but then the mutation of ten amino acids in this helix resulted in a breakdown of the whole helix. Surprisingly a new orientation of the GLU 336 side chain back to the HIS 449 was observed. Also the deformation of this counter helix induces unfolding of the entrance helix.

We assume that the sequence of these ten amino acids is crucial for the access of the substrates to the active site of PLE, determining the shape of the entrance channel together with the entrance helix (72-87). It thus seems to be possible that the evolution of the entrance channel in PLE induced a reorientation of the GLU 336 side chain away from the active site, being replaced by the GLU 452 carboxyl group.

Conclusions

Simulations for more than 10 ns are sufficient to change local conformations and thus to reveal significant differences between the enzyme and its template for homology modeling. In one case the simulation time was even sufficient for modifying the fold of a heptapeptide. Unrestrained runs result in stable structures with well defined active sites. Reliable models are obtained for enzymes, for which no experimental structural data are available. The stability of the trimer in the simulation and the identification of contacts between its monomers are a further validation of the simulation.

Our enzyme model provides a rigid carapace made up from β-strands and a **soft body** of α-helices containing the mutations and determining the experimental substrate specificity. Similar to hCE the access of the substrate to the active site passes through two α-helices. Their structure and even the folding state of one of them are specifically affected by mutations which modify the substrate specificity. This makes it likely that the entrance channel rather than the structure of the active site determines the substrate specificity of the enzyme.

In addition to that it was shown that the exchange of the GLU residue within the families of hydrolases is not essential for the reaction mechanism as long as the composition of the triad is conserved. This model of enzyme specificity sheds a new light on the mechanisms of esterase reactions and on the possibilities to tailor substrate specific enzymes.

Acknowledgments

We gratefully acknowledge support of Markus Gall (Institute of Biochemistry, Greifswald) for an introduction into the 3DM database, and fruitful discussions with Dr. Elke Brüsehaber, Anke Hummel and Dr. Robert Kourist (Institute of Biochemistry, Greifswald).

References

1. Bornscheuer UT, Kazlauskas RJ (2005) Hydrolases in organic synthesis. 2nd edn. Wiley-VCH
2. de Maria PD, Garcia-Burgos CA, Bargeman G, van Gemert RW (2007) Pig liver esterase (ple) as biocatalyst in organic synthesis: From nature to cloning and to practical applications. Synthesis-Stuttgart 10:1439-1452. doi:10.1055/s-2007-966024
3. Sussman JL, Harel M, Frolow F, Oefner C, Goldman A, Toker L, Silman I (1991) Atomic-structure of acetylcholinesterase from torpedo-californica - a prototypic acetylcholine-binding protein. Science 253:872-879
4. Shafferman A, Kronman C, Flashner Y, Leitner M, Grosfeld H, Ordentlich A, Gozes Y, Cohen S, Ariel N, Barak D, Harel M, Silman I, Sussman JL, Velan B (1992) Mutagenesis of human acetylcholinesterase - identification of residues involved in catalytic activity and in polypeptide folding. J Biol Chem 267:17640-17648
5. Monecke P, Friedemann R, Naumann S, Csuk R (1998) Molecular modelling studies on the catalytic mechanism of candida rugosa lipase. J Mol Model 4 (12):395-404
6. Bencharit SM, Christopher L, Howard-Williams, Escher L, Danks MK, Poter PM, Redinbo MR (2002) Structural insights into cpt-11 activation by mammalian carboxylesterases. Nat Struct Biol 9:6
7. Ollis DL, Cheah E, Cygler M, Dijkstra B, Frolow F, Franken SM, Harel M, Remington SJ, Silman I, Schrag J, Sussman JL, Verschueren KHG, Goldman A (1992) The alpha/beta-hydrolase fold. Protein Eng 5:197-211
8. Heymann E, Mentlein R, Schmalz R, Schwabe C, Wagenmann F (1979) Method for the estimation of esterase synthesis and degradation and its application to evaluate the influence of insulin and glucagon. Eur J Biochem 102:509-519
9. Junge W, Heymann E (1979) Characterization of the isoenzymes of pig-liver esterase .2. Kinetic studies. Eur J Biochem 95:519-525
10. Musidlowska A, Lange S, Bornscheuer UT (2001) By overexpression in the yeast pichia pastoris to enhanced enantioselectivity: New aspects in the application of pig liver esterase. Angew Chem Int Ed 40:2851-2853
11. Bottcher D, Brusehaber E, Doderer K, Bornscheuer UT (2007) Functional expression of the gamma-isoenzyme of pig liver carboxyl esterase in escherichia coli. Appl Microbiol Biotechnol 73:1282-1289. doi:10.1007/s00253-006-0585-1

12. Hummel A, Brusehaber E, Bottcher D, Trauthwein H, Doderer K, Bornscheuer UT (2007) Isoenzymes of pig-liver esterase reveal striking differences in enantioselectivities. Angew Chem Int Ed 46:8492-8494. doi:10.1002/anie.200703256
13. Hummel A (2007) Identifizierung von isoenzymen der schweineleberesterase. Ernst-Moritz-Arndt-Universität, Greifswald (Diploma Thesis)
14. Hermann M, Kietzmann MU, Ivancic M, Zenzmaier C, Luiten RGM, Skranc W, Wubbolts M, Winkler M, Birner-Gruenberger R, Pichler H, Schwab H (2008) Alternative pig liver esterase (aple) - cloning, identification and functional expression in pichia pastoris of a versatile new biocatalyst. J Biotechnol 133:301-310. doi:10.1016/j.jbiotec.2007.10.010
15. Bencharit S, Morton CL, Xue Y, Potter PM, Redinbo MR (2003) Structural basis of heroin and cocaine metabolism by a promiscuous human drug-processing enzyme. Nat Struct Biol 10:349-356. doi:10.1038/nsb919
16. Gasteiger E, Gattiker A, Hoogland C, Ivanyi I, Appel RD, Bairoch A (2003) Expasy: The proteomics server for in-depth protein knowledge and analysis. Nucleic Acids Res 31:3784-3788. doi:10.1093/nar/gkg563
17. Bencharit S, Morton CL, Hyatt JL, Kuhn P, Danks MK, Potter PM, Redinbo MR (2003) Crystal structure of human carboxylesterase 1 complexed with the alzheimer's drug tacrine: From binding promiscuity to selective inhibition. Chem Biol 10:341-349. doi:10.1016/s1074-5521(03)00071-1
18. Case DA, Darden TA, Cheatham TE, Simmerling CL III,, Wang J, Duke RE, Luo R, Crowley M, Walker Ross C, Zhang W, Merz KM, Wang B, Hayik S, Roitberg A, Seabra G, Kolossváry I, Wong KF, Paesani F, Vanicek J, Wu X, Brozell SR, Steinbrecher T, Gohlke H, Yang L, Tan C, Mongan J, Hornak V, Cui G, Mathews DH, Seetin MG, Sagui C, Babin V, Kollman PA (2008) AMBER 10. University of California, San Francisco
19. Humphrey W, Dalke A, Schulten K (1996) Vmd: Visual molecular dynamics. J Mol Graph 14:33-&
20. Stone J (1998) An efficient library for parallel ray tracing and animation. Master, University of Missouri-Rolla, (Master Thesis)
21. Frishman D, Argos P (1995) Knowledge-based protein secondary structure assignment. Protein Struct Funct Gen 23:566-579
22. Eargle J, Wright D, Luthey-Schulten Z (2006) Multiple alignment of protein structures and sequences for vmd. Bioinformatics 22:504-506. doi:10.1093/bioinformatics/bti825

23. Gille C, Frommel C (2001) Strap: Editor for structural alignments of proteins. Bioinformatics 17:377-378
24. Musidlowska-Persson A, Bornscheuer UT (2003) Site directed mutagenesis of recombinant pig liver esterase yields mutants with altered enantioselectivity. Tetrahedron: Asymmetry 14:4
25. Lange S, Musidlowska A, Schmidt-Dannert C, Schmitt J, Bornscheuer UT (2001) Cloning, functional expression, and characterization of recombinant pig liver esterase. ChemBioChem 2:576-582
26. Hass MAS, Hansen DF, Christensen HEM, Led JJ, Kay LE (2008) Characterization of conformational exchange of a histidine side chain: Protonation, rotamerization, and tautomerization of his61 in plastocyanin from anabaena variabilis. J Am Chem Soc 130:8460-8470. doi:10.1021/ja801330h
27. Schrag JD, Li Y, Wu S, Cygler M (1991) Ser-his-glu triad forms the catalytic site of the lipase from geotrichum-candidum. Nature 351:761-764
28. Manco GM, Mosè L, Mosè R (2001) Residues at the active site of the esterase 2 from alicyclobacillus acidocaldarius involved in substrate specificity and catalytic activity at high temperature. J Biol Chem 276:9
29. Hosokawa M (2008) Structure and catalytic properties of carboxylesterase isozymes involved in metabolic activation of prodrugs. Molecules 13:412-431
30. Cygler M, Schrag JD, Sussman JL, Harel M, Silman I, Gentry MK, Doctor BP (1993) Relationship between sequence conservation and 3-dimensional structure in a large family of esterases, lipases, and related proteins. Protein Sci 2:366-382

Tables

Table 1 Differences in the sequences of the PLE- isoenzymes. For PLE1 all residues are shown, which undergo mutations in any of the other isoenzymes. In the other columns, only exchanged residues are indicated,"–" means no change with respect to PLE1. Three letter code is used for the amino acids. Groups of correlated mutations are indicated (see text)

Group	Residue	PLE1	PLE2	PLE3	PLE4	PLE5	PLE6	APLE
(1)	73	ASP	-	GLU	-	-	GLU	GLU
	75	VAL	-	ILE	-	-	ILE	ILE
	76	VAL	-	GLY	ALA	ALA	GLY	GLY
	77	GLU	-	GLY	GLY	GLY	GLY	GLY
	80	THR	-	LEU	-	-	LEU	LEU
(2)	87	GLY	-	ARG	ARG	ARG	ARG	ARG
	92	THR	-	ILE	ILE	ILE	ILE	ILE
	93	LEU	-	PRO	PRO	PRO	PRO	PRO
	129	LEU	-	VAL	VAL	VAL	VAL	VAL
	133	PRO	-	SER	SER	SER	SER	SER
	134	MET	-	THR	THR	THR	THR	THR
	138	VAL	-	LEU	LEU	LEU	LEU	LLEU
	139	VAL	-	ALA	ALA	ALA	ALA	ALA
	234	LEU	-	PHE	PHE	PHE	PHE	PHE
	236	VAL	-	ALA	ALA	ALA	ALA	ALA
	237	ALA	-	GLY	GLY	GLY	GLY	GLY
(3)	285	PHE	-	PRO	PRO	-	-	-
(4)	286	LEU	-	-	-	PHE	PHE	PHE
	287	THR	-	-	-	ALA	ALA	ALA
(5)	290	PHE	-	LEU	LEU	LEU	LEU	LEU
	294	GLN	-	PRO	PRO	PRO	PRO	PRO
	302	PRO	-	THR	THR	THR	THR	THR
(6)	459	PHE	ALA	-	ALA	ALA	ALA	-
	461	LEU	PHE	-	PHE	PHE	PHE	-
	463	LYS	ARG	-	ARG	ARG	ARG	-

Table 2a Residues linking the monomer subunits 1-3 to its neighbor in clockwise sense. Connections are found between 1 and 5' (cf. Table 2b) (*cyan – red* in Fig. 8), 2 and 6' (*blue – orange*), the first 2 amino acids of 2 and 7' (*blue – orange*), the remaining amino acids of 2 and 4' (*blue – yellow*) and between 3 and 5' (*iceblue – red*). Only the SER 45 (*magenta*) and GLU 270 residues (*cyan*) of each of the three monomers in the center of the structure form contacts to the two other subunits both in clockwise and counterclockwise sense. Colors refer to Fig. 8.

Amino acid	Number	contacts su1 to su2	contacts su2 to su3	contacts su3 to su1
SER	45	X	X	X
strand 1 (*cyan*)				
ASP	165	X	X	X
GLU	166	X	X	X
HIS	167	X	X	X
ARG	169	X	X	
strand 2 (*blue*)				
LYS	257	X	X	X
THR	259	X	X	X
THR	260	X	X	X
ALA	262	X	X	X
VAL	263	X	X	X
HIS	266	X	X	X
ARG	269	X	X	
GLU	270	X	X	X
strand 3 (*iceblue*)				
VAL	305	X		X
ASP	306	X		X
GLY	307	X	X	X
VAL	308	X	X	X

Tab 2b Residues linking the monomer subunits 1-3 to its neighbor in counterclockwise sense

Amino acid	Number	contacts su1 to su3	contacts su3 to su2	contacts su2 to su1
strand 4‘ (*yellow*)				
PRO	41	X	X	
LEU	43	X	X	X
GLY	44	X	X	
SER	45	X	X	X
ARG	47	X	X	
strand 5‘ (*red*)				
GLU	55	X	X	X
PRO	56	X	X	X
TRP	57	X	X	X
SER	58	X	X	X
PHE	59	X	X	X
LYS	61	X	X	X
ASN	62		X	X
PRO	68	X	X	X
strand 6‘ (*orange*)				
GLU	94	X	X	X
PHE	95	X	X	X
SER	96	X	X	X
GLU	97	X	X	
ASP	98	X	X	X
TYR	101	X	X	X
strand 7‘ (*orange*)				
GLU	270	X	X	X
SER	272	X		X

Tab 3a Residues in the active site: Hydrogen bonding of SER 204 analogs in selected hydrolases

Enzyme	Serin	Atom	H-bond acceptor	Remarks
Pig liver esterase	204	OG	HIS 449 NE2	active site (mostly stable)
	204	OG	GLU 229 O	alternative
Human Carboxyl-esterase I	201	OG	HIS 447 NE2	active site
		OG	GLU 200 OEX	alternative
Torpedo californica Acetylcholinesterase	197	OG	HIS 437 NE2	active site (stable)
Human Butyrylcholinesterase	196	OG	HIS 436 NE2	active site (not stable)
			SER 222 O	alternative (more stable)
Candida rugosa lipase	209	OG	HIS 449 NE2	active site (mostly stable)
	209	OG	GLY 123 O	alternative

Tab 3b Bonding of the residue GLU 333 and its ASP/GLU analogs in selected hydrolases

Enzyme	ASP/GLU	Atom	H-bond donor	Remarks
Pig liver esterase	336	OEX	GLU 336 N	oriented away from the active site (stable)
	336	OEX	LYS 521 NZ	(stable)
Human Carboxyl-esterase I	334	OEX	GLU 334 N	oriented away from the active site
	334	OEX	LYS 519 NZ	
Torpedo californica Acetylcholinesterase	324	OEX	HIS 437 ND1	part of the active site (stable)
	324	OEX	ASN 321 N	(stable)
	324	OEX	SER 223 OG	
Human Butyrylcholinesterase	323	OEX	HIS 436 ND1	part of the active site (stable)
	323	OEX	SER 222 OG	
	323	OEX	ASN 320 ND	
	323	OEX	ASN 320 N	
Candida rugosa lipase	341	OEX	HIS 449 ND1	part of the active site (stable)
	341	OEX	SER 241 OG	
	341	OEX	GLN 338 N	

Table 3c Bonding of the residue GLU 449 and its ASP/GLU analogs in selected hydrolases

Enzyme	ASP/GLU	Atom	H-bond donor
Pig liver esterase	452	OEX	HIS 449 ND1
	452	OEX	SER 230 OG
	452	OEX	GLY 450 N
	452	OEX	ASP 451 N
	452	OEX	GLU 452 N
Human Carboxyl-esterase I	450	OEX	HIS 447 ND1
	450	OEX	ASN 331 ND2
	450	OEX	GLY 448 N
	450	OEX	ASP 449 N
Torpedo californica Acetylcholinesterase	440	OEX	GLN 222 NE2
	440	OEX	ASN 321 ND2
	440	OEX	TYR 418 OH
Human Butyrylcholinesterase	439	OEX	ASN 320 ND2
	439	OEX	GLN 221 NE2
Candida rugosa lipase	452	ODX	GLN 338 OE1
	452	ODX	SER 436 OG
	452	ODX	GLN 438 NE2
	452	ODX	TYR 467 OH

Figure captions

Fig. 1 Structure of the enzyme PLE1: α-helices, β-strands and random coils are indicated in *yellow*, *magenta* and *cyan*, respectively

Fig. 2 Steric view of the mutations transferring PLE1 to the other isoenzymes. The helix consisting of residues 72-83 and the five mutations inside the helix are shown in *green* and *purple*, respectively. Five mutations within 5 Å from the helix, six between 5 Å and 7 Å and nine more than 7 Å away are presented in *yellow*, *orange* and *red*, respectively

Fig. 3 Plots of the RMSD of selected amino acids of PLE 3 as a function of simulation time

a Residues 438 – 444 in a loop. Symbols denote data; full lines indicate single exponential decays. (*Traces are shifted in +y direction according to the numbers indicated in brackets in the legend*). The RMSD relaxes from about 7 to 2 Å. This indicates stress on the initial structure due to the introduction of mutations. A small oscillation is superposed to the relaxation

b Residues 459 – 463 in a 3_{10}-helix: (*Traces shifted as in* **a**) The fits indicate an oscillation of 1 to 2 Å amplitude and 200 MHz frequency. This seems to be due to thermal motion rather than to relaxation from stress

Fig. 4 Cartoon plot of PLE1 indicating soft and rigid parts of the structure. The β-folds and a few α-helices have average RMSD in PLE2-6 and APLE with respect to monomer PLE1 of less than 2 Å (*yellow*). The majority of the α-helices form a contiguous front part of the enzyme with RMSD values from 2 up to 14 Å. The four residues (204, 449, 452, 336) of the active site are indicated by red vdW spheres. The entrance helix, (72-87), and the opposite helix, (338-346), (*both marked by black lines*) clearly surround the access to the active site

Fig. 5 Snapshots of sterical structured of the entrance helix, (72-87), after 14 ns of simulation time

a Superposition of the structures for the isozymes PLE1 (*blue*), PLE2 (*red*) , PLE3 (*yellow*) , PLE4 (*green*), PLE5 (*cyan*), PLE6 (*magenta*), and APLE (*lime*). Significant differences between these structures are seen

b as **a**, but only PLE1 and PLE3. Ball and stick presentation of the amino acids is added, corresponding residues have identical colors. Partial unfolding of PLE3 is clearly seen

Fig. 6 Ramachandran plots for final structures of the residues 74 to 83 in the range of the entrance helix

For PLE1 (*left*) the positions of nearly all residues are in the typical range of the α-helix, whereas in PLE3 (*right*) several residues are outside this range

Fig. 7 Structure of residues (89-96) close to the entrance helix only PLE1: Superposition of frames after 0, 4, 8, 12 and 14 ns (*blue*, *red*, *yellow*, *green* and *purple*, respectively). The sequence shows folding and unfolding during the simulation time

Fig. 8 Structure of the PLE1 trimer *from the top*. Residues in contacts to the neighboring monomer are marked by van der Waals-spheres. *Yellow* and *dark blue* zones indicate contacts to the next monomer in clockwise and counter clockwise sense. The insert shows the contact between subunits 1 and 2 (*view from the bottom*). Strands forming the contact are colored according to Table 3

Fig. 9 Time history of characteristic atom-atom distances in the active site of the PLE1 monomer during the molecular dynamics run. The *black line* indicates high stability of the SER204-HIS449 hydrogen bond. In competition to this interaction, the serine residue forms hydrogen bonds to the backbone oxygen atoms of the glutamic acids 203 and 229 (cf. Table 3a)

Fig. 10 Aligned sequences of the complete PLE1, the PLE1 with clipped ends as obtained from homology modeling, and the mutations of residues 337-346, which affected the folding of the entrance helix (see text). Cysteins involved in cystin bridges are labeled as X rather than C

Figure 1

Click here to download high resolution image

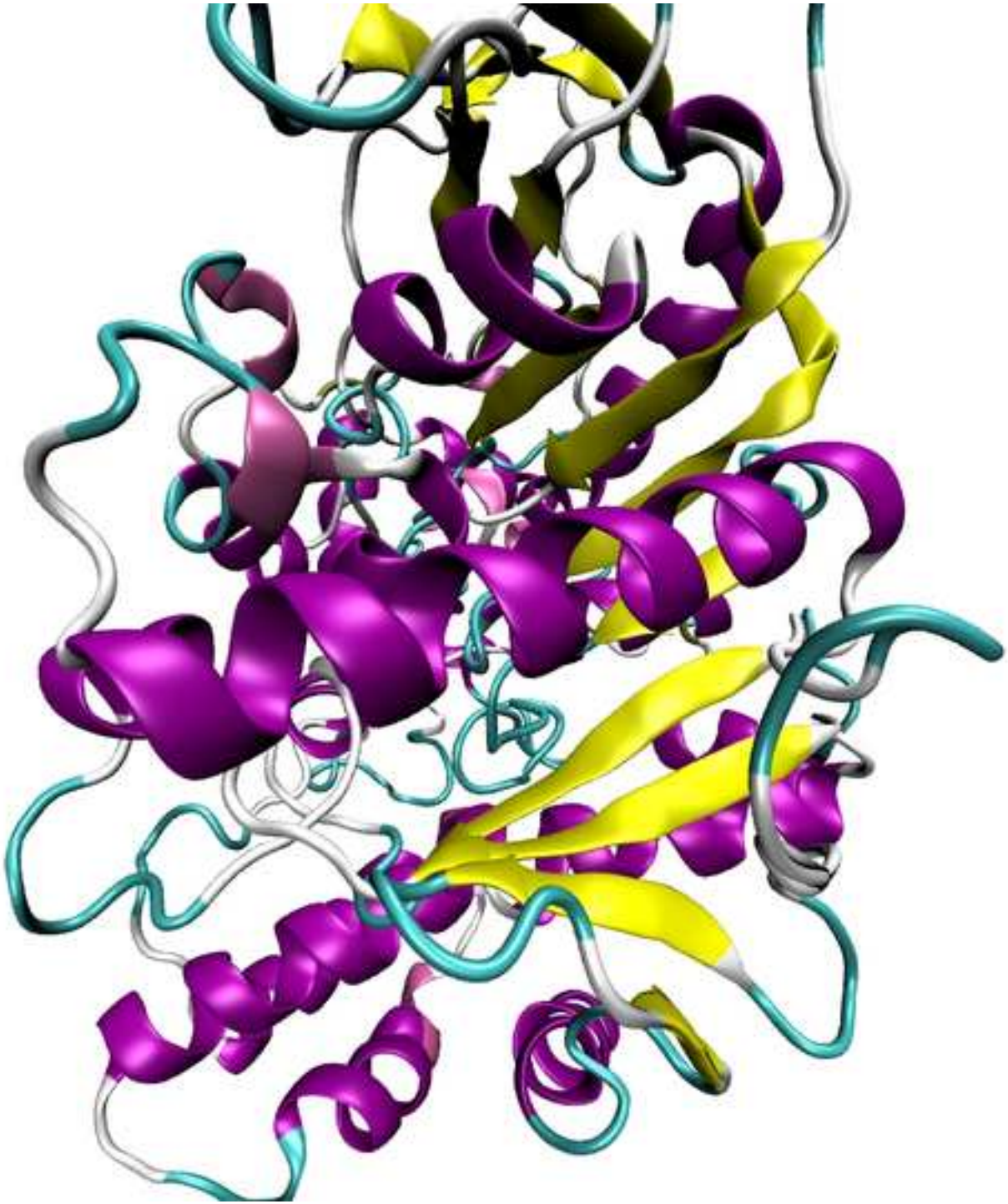

Figure 2
Click here to download high resolution image

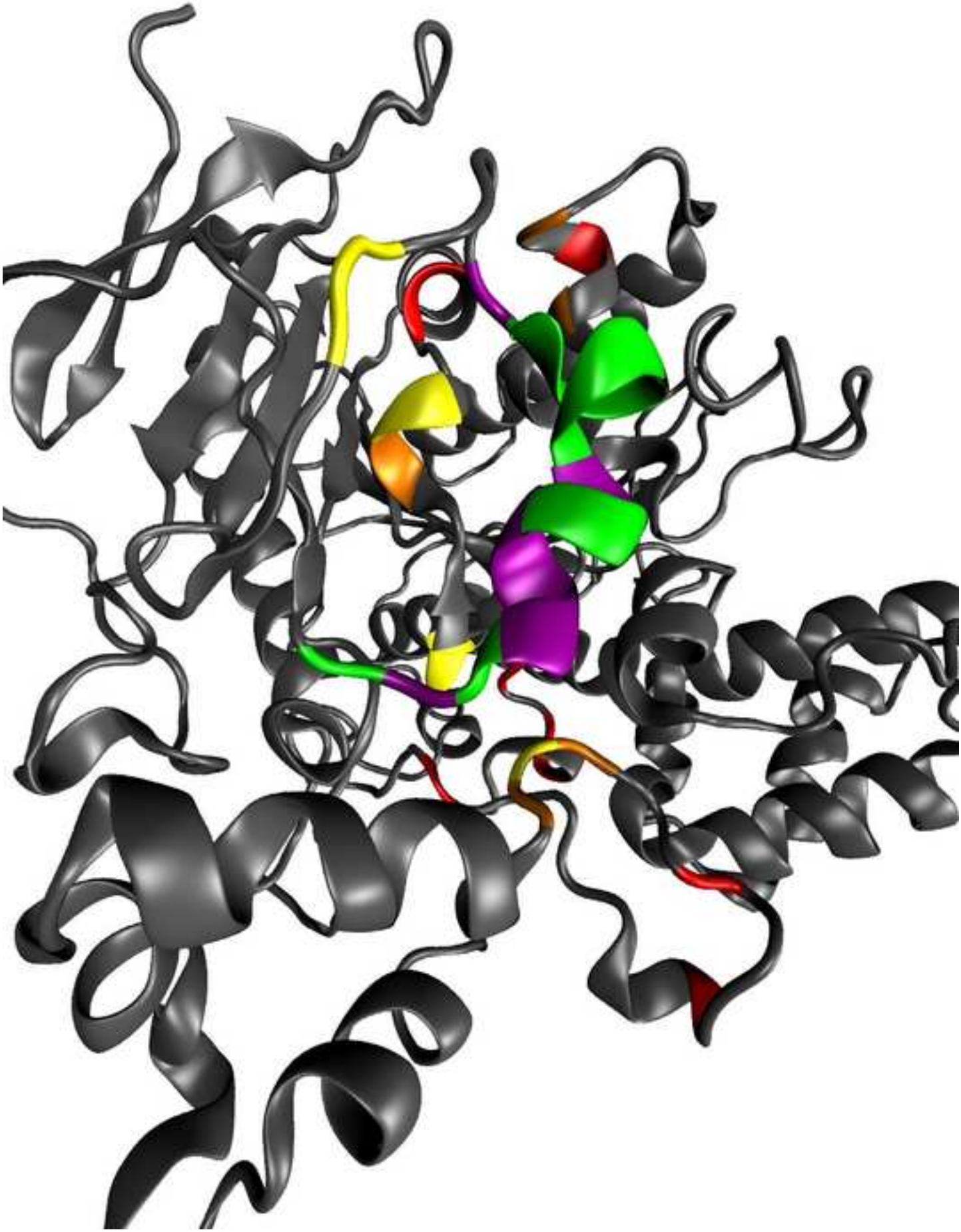

Figure 3a

Click here to download high resolution image

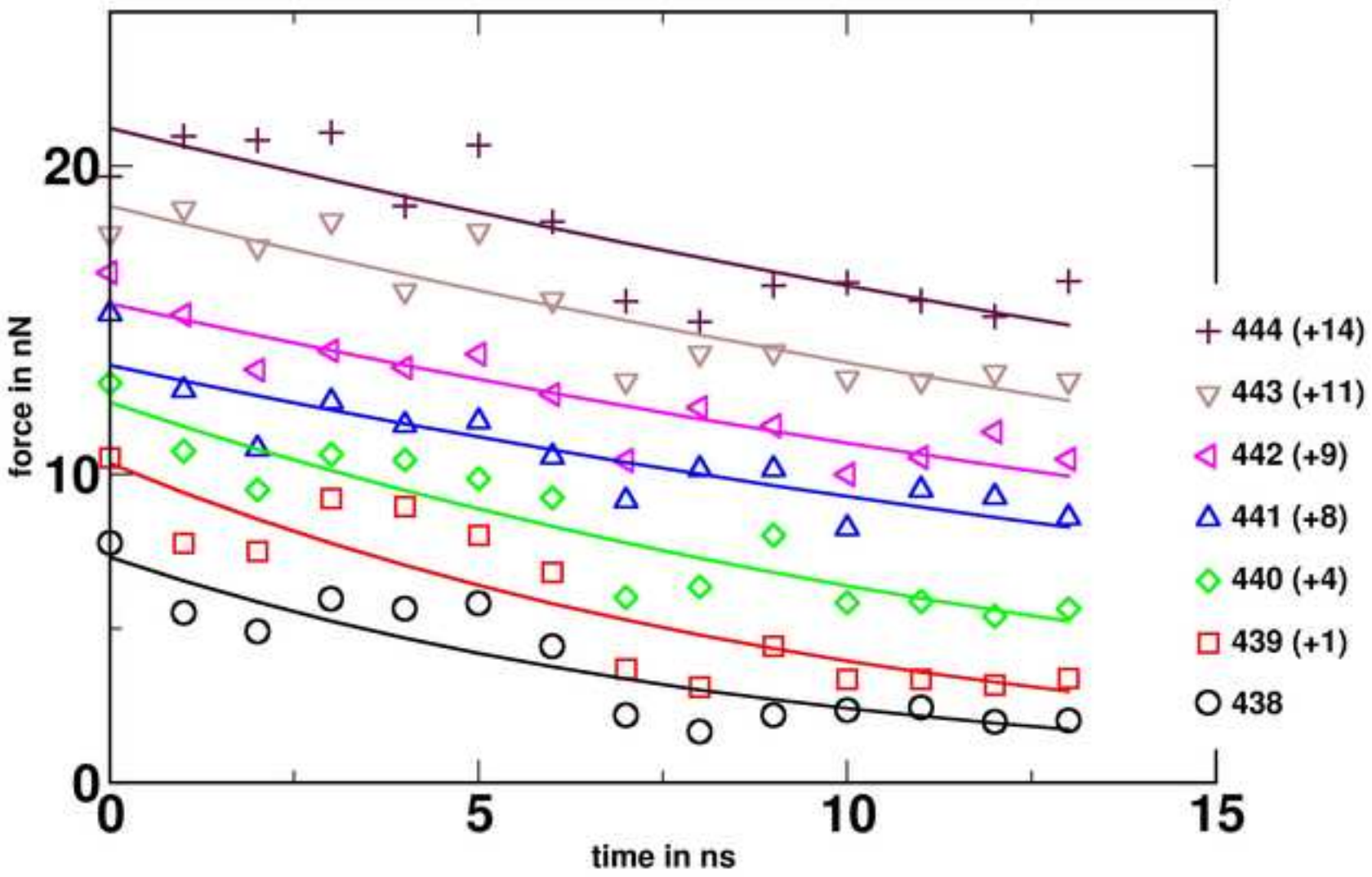

Figure 3b
Click here to download high resolution image

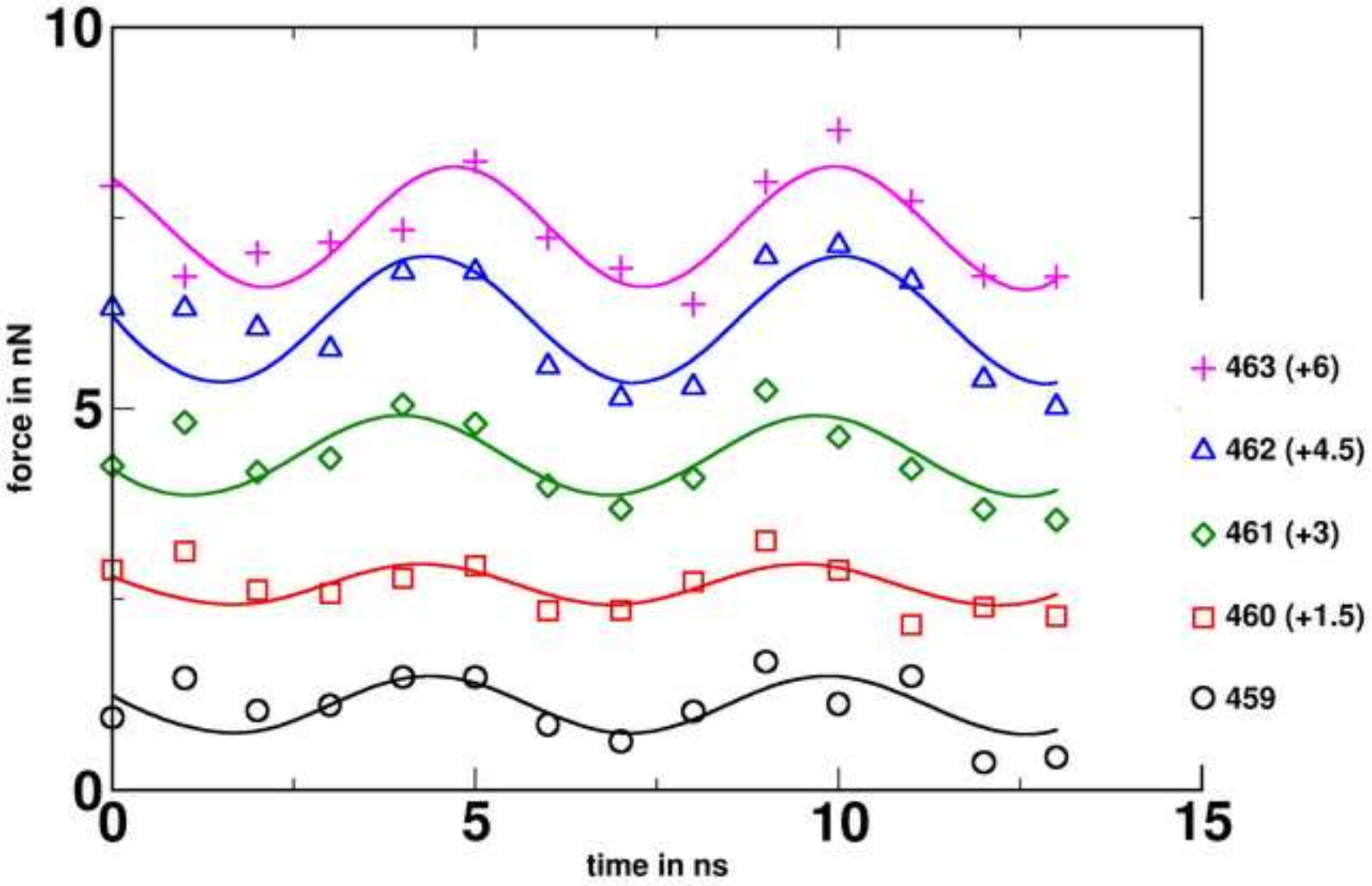

Figure 4

Click here to download high resolution image

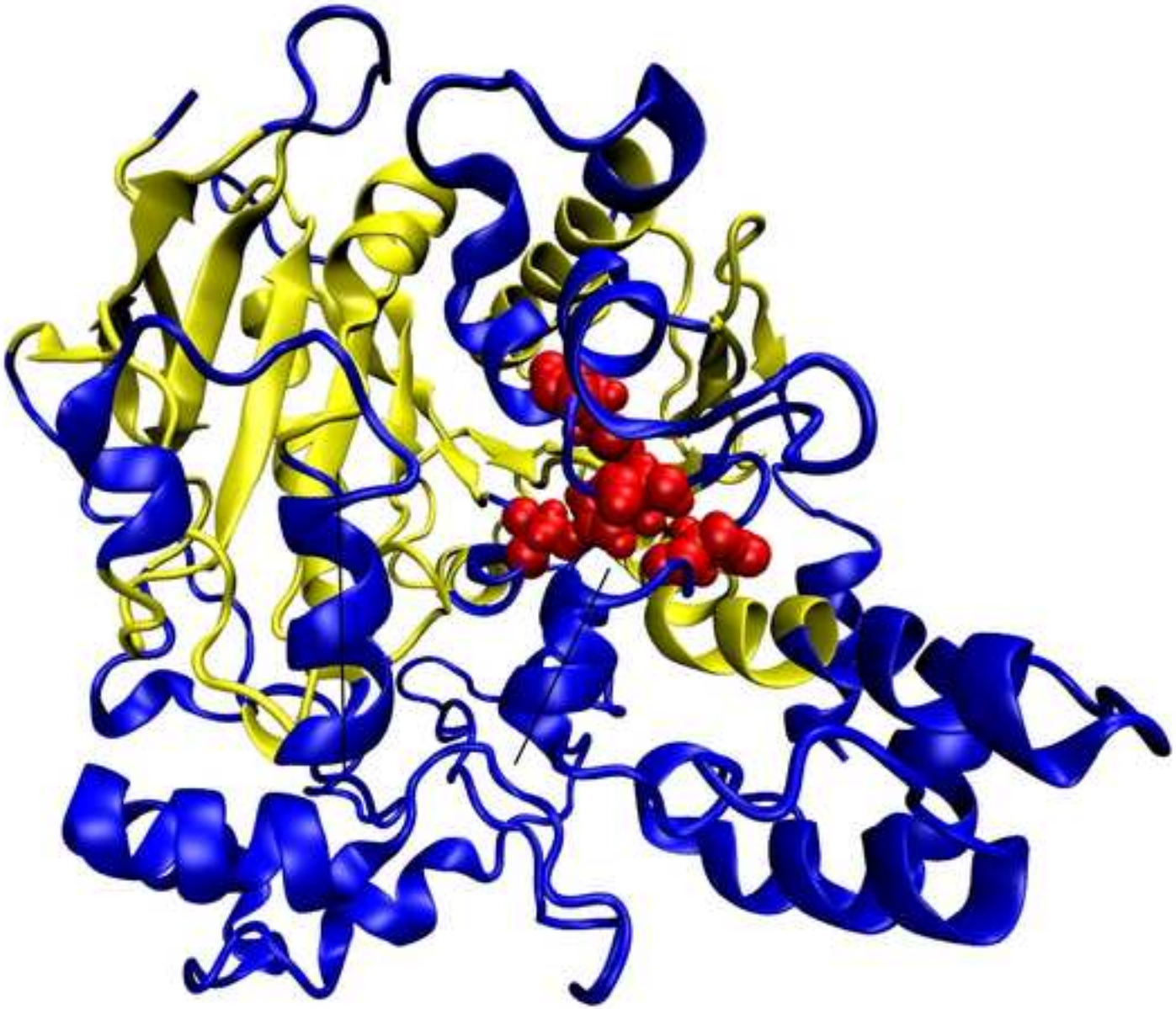

Figure 5a
Click here to download high resolution image

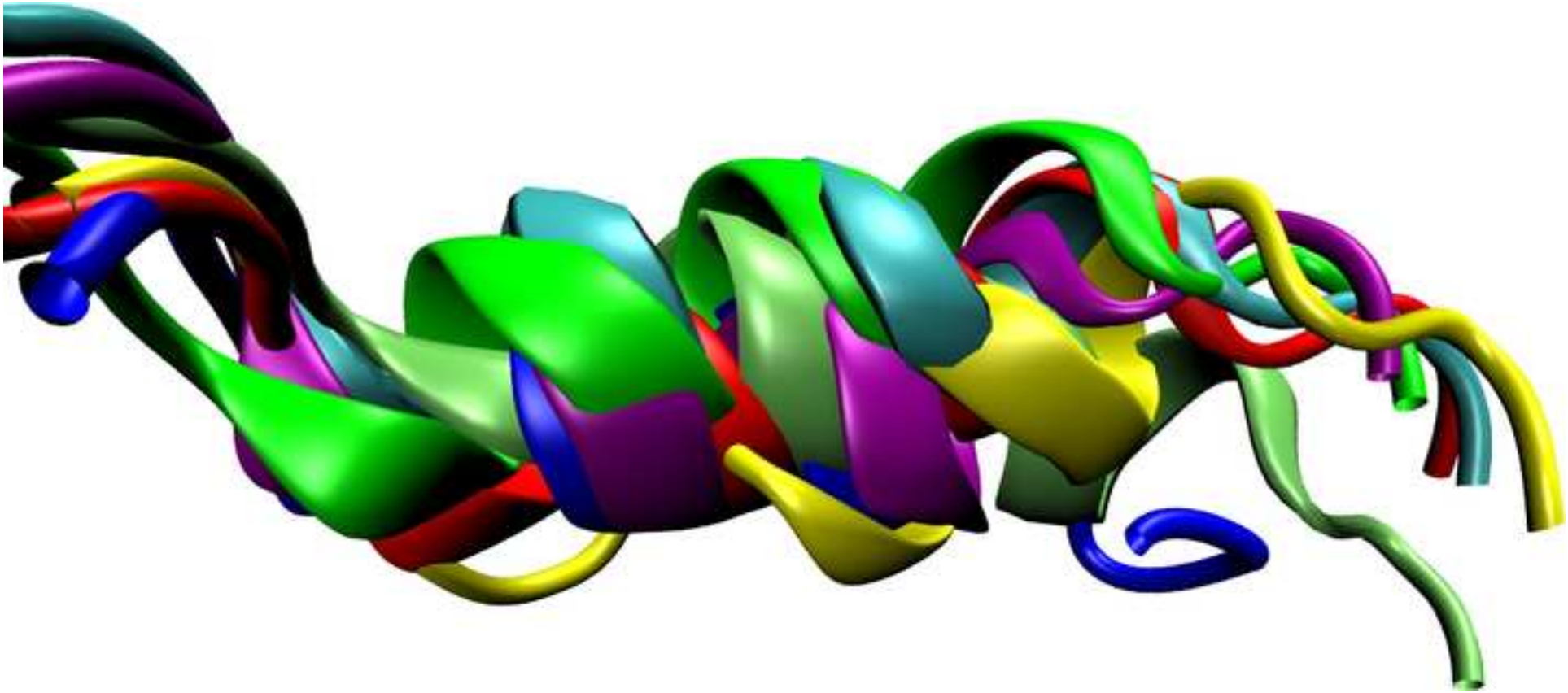

Figure 5b

Click here to download high resolution image

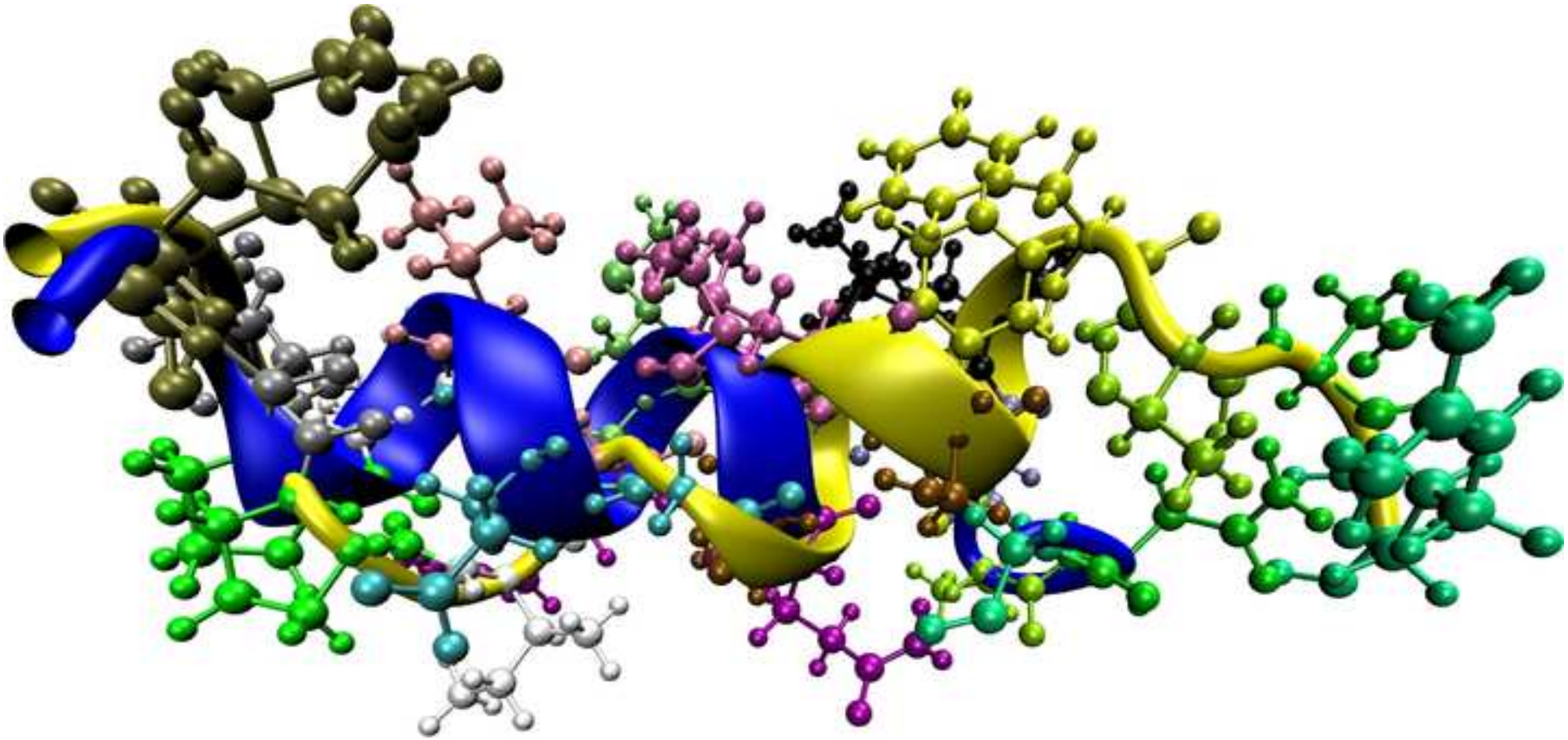

Figure 6

Click here to download high resolution image

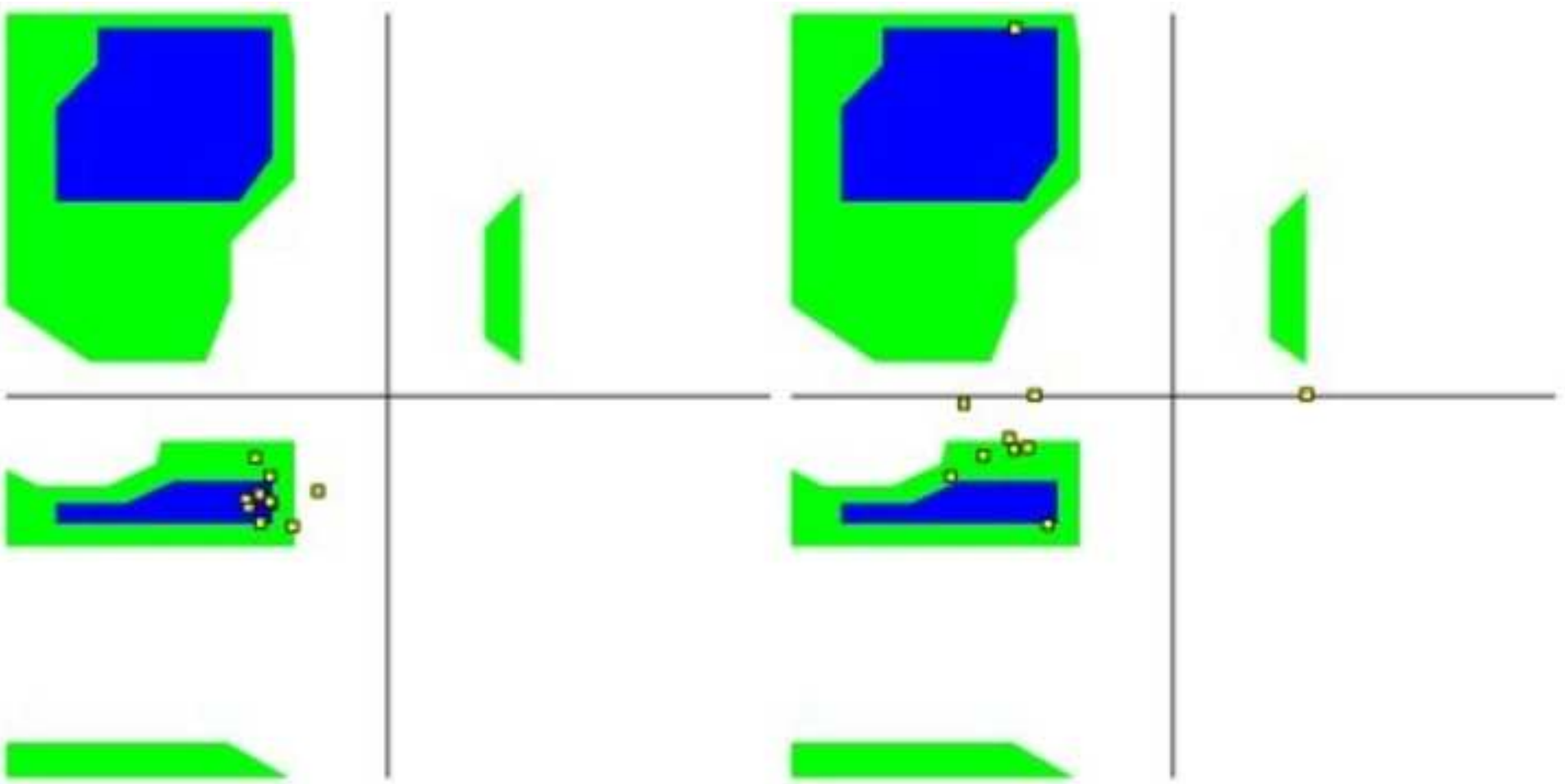

Figure 7
Click here to download high resolution image

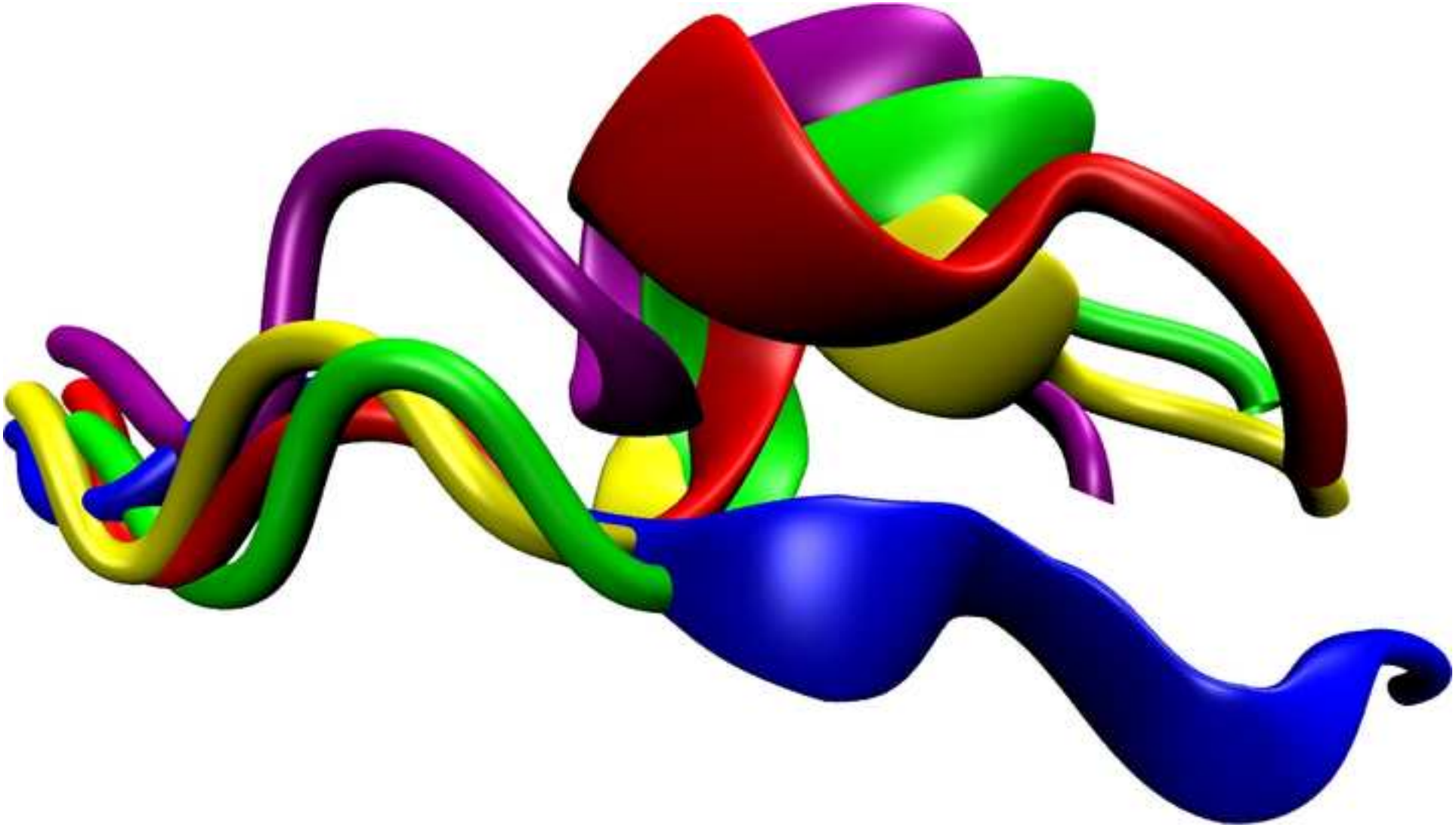

Figure 8

Click here to download high resolution image

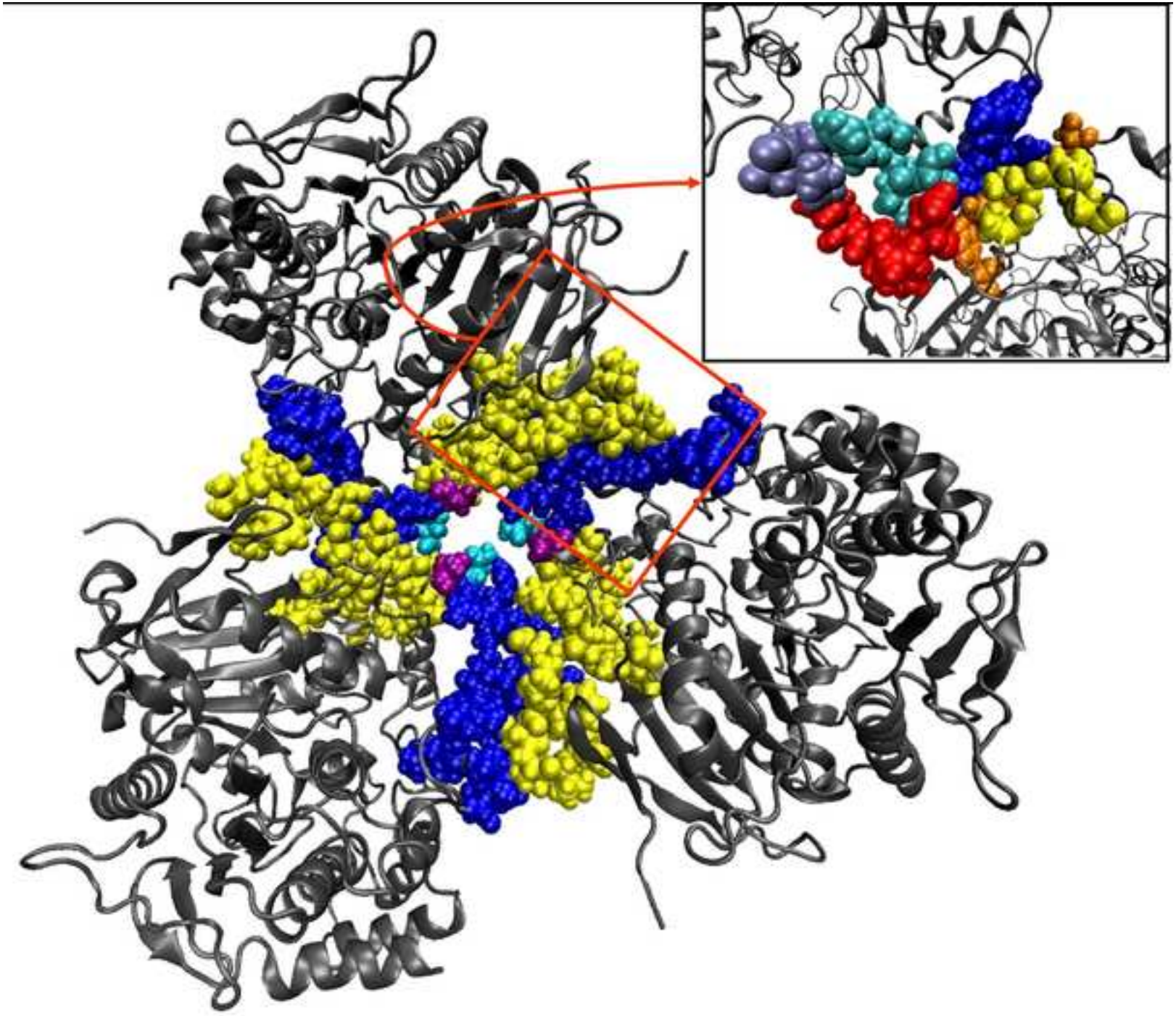

Figure 9

Click here to download high resolution image

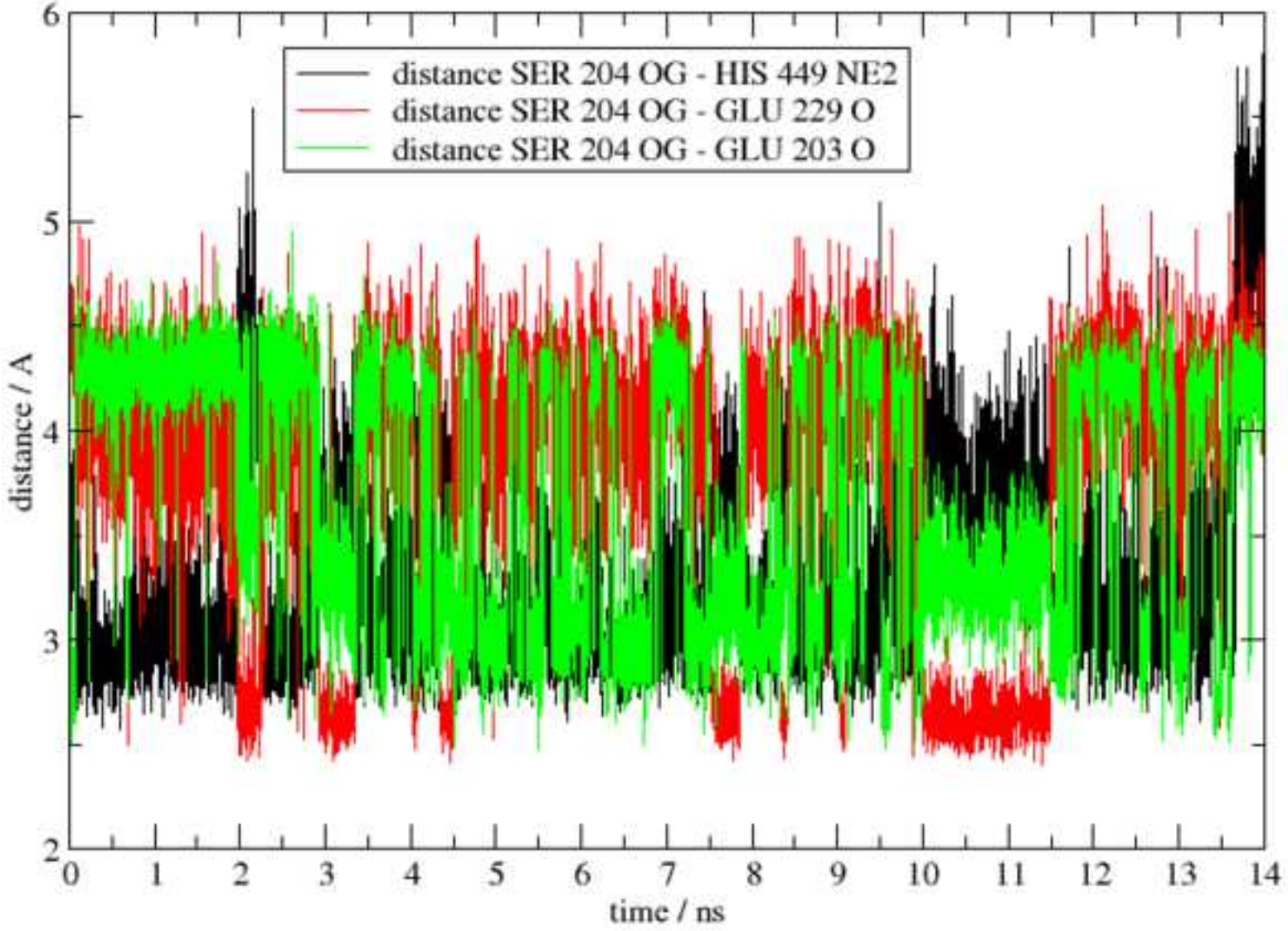

Figure 10

Click here to download high resolution image